ANALYSIS OF AN AUTOPILOT WITH SATURATING TYPE NONLINEAR ELEMENT

by

CLYDE HOWARD SPRAGUE

B. S., Kansas State University, 1958

A MASTER'S THESIS

submitted in partial fulfillment of the

requirements for the degree

MASTER OF SCIENCE

Department of Mechanical Engineering

KANSAS STATE UNIVERSITY
Manhattan, Kansas

1963

Approved by: Ralph A. Flores

Major Professor

TABLE OF CONTENTS

INTRODUCTION

The era subsequent to the last World War has seen tremendous technological strides in the fields of manned and unmanned flights. Manned flights of aerodynamic and hybrid vehicles have extended to speeds of several times that of sound and to altitudes of tens of miles. Control of these vehicles has long since passed the stage of direct control and fly by feel. Very sopisticated control systems are used to aid the pilot in manned flight and to completely control the vehicle in the case of unmanned flights.

One of the important subsystems in these sophisticated flight control systems is the automatic pilot or autopilot. It is the function of the autopilot to carry out precisely the maneuvers called for by the guidance system. Coupled together, the autopilot and guidance system direct the vehicle along the trajectory required to intercept the target. Accuracy, speed, and stability are three prime requirements for a good autopilot.

In the missile field, vehicles of extremely high speed and altitude capabilities have been developed. These vehicles require control systems which are extremely fast and which have very broad dynamic ranges. To meet this severe demand on the control system and in particular on the autopilot the use of intentionally introduced nonlinear elements is often considered.

A typical nonlinear element is one which has only two possible states, fully on in either of two directions. Such devices usually simplify the

system hardware but almost always complicate the analysis. Superposition is no longer permissible and analysis for one type of signal does not always yield useful information about other types. The merits of such systems, however, more than offset the difficulty of analysis.

The analysis of a simple nonlinear control system for an aerodynamic vehicle is undertaken in this paper. The primary objectives of the work to follow are to show a means of analyzing a system of this type and to indicate a design procedure for a fixed parameter system. For a simple system amenable to a direct literal analysis, a complete design is undertaken. It is shown that air data scheduling is not required to achieve a stable system with adequate response throughout the flight regime if a two state nonlinearity is used.

For any aerodynamic configuration the effectiveness of the control surfaces in changing the flight path is a function of the Mach number and the local static pressure. Hence, the control system must cope with a vehicle whose equations of motion are strong functions of the local dynamic pressure. Typical flights may encompass a range of dynamic pressure of ten to a hundred depending on the vehicle and the trajectory. This fact alone precludes the use of a fixed parameter linear system. As a consequence, early linear control systems compensated for dynamic pressure variations by elaborate use of air data measurements. Mach number and local static pressure were continuously measured (usually by measuring ram pressure) and these data used to vary the control system parameters.

To design a system of the above type, one must have accurate knowledge of the airframe transfer function for all dynamic pressures and all trim conditions. Furthermore, the hardware necessary to accomplish the gain scheduling is quite complicated and often unreliable. Use of nonlinear control as suggested in this paper, obviates the need for air data scheduling equipment and at the same time yields an autopilot which has a response superior to a linear system.

SYSTEM DESCRIPTION

The functional block diagram of a typical guided missile control system is shown in Fig. 1. In any such system the target and missile positions in space are compared and the resultant guidance error signal is fed to the missile control system which in turn acts to null the error signal. Clearly, the particular method of guidance error detection is determined by the type of guidance system used. For example, a beam-riding system employs a separate guidance and tracking radar whereas a homing system employs a missile bound seeker unit. The type of guidance system used will also determine the basic nature of the guidance error signal.

The guidance computer is used to provide the appropriate error signal gain and shaping to convert the error signal to a suitable missile lateral acceleration command signal; thus its form is determined by the type of guidance. The missile autopilot in turn accepts the acceleration command signal and activates the control surfaces as required to provide this desired lateral acceleration. The component of this lateral

acceleration, which is normal to the flight path acting in conjunction with the missile velocity, produces a change in flight path angle so as to null the error between the desired missile position in space (the target position) and the actual position.

That portion of the missile system which constitutes the autopilot is enclosed in dashed lines in Fig. 1. It is this portion of the system which will be of concern for the remainder of this paper. The airframe considered in this study uses small control surfaces located remotely from the missile center of gravity to achieve large turning moments. Lift or lateral acceleration forces are derived primarily from the missile body and thus are due primarily to angle of attack. Normal forces resulting from control surface deflection are small relative to the body forces and are thus neglected.

The airborne portion of a missile control system must maintain control of the three airframe coordinates; pitch, yaw, and roll. Generally, the roll system functions only to stabilize the roll angle. A roll free gyro and a roll rate gyro are used in conjunction with appropriate feedback networks to stabilize the roll angle (i.e., the roll system maintains a prescribed roll orientation throughout the flight). For purposes of this study, it is assumed that separate moment or force devices are provided for the roll system. This essentially divorces the roll and steering systems so that they may be treated as distinct systems.

The pitch and yaw planes are essentially identical and independent in the absence of roll-yaw-pitch (RYP) coupling through the aerodynamics and thus treatment of one plane suffices for both. Maneuvers in either

plane or in any combined plane are permissible with the latter being a linear combination of the single plane motions. Separate sensing instruments are provided for each plane.

Standard pitch plane nomenclature is shown in Fig. 2. In the discussion to follow, the terms pitch, yaw, and steering refer to lateral motions or planes of motion and are used synonomously. In Fig. 1, the autopilot is assumed to be an "acceleration feedback" (AFB) system wherein the command acceleration is compared with the actual missile acceleration as measured by an accelerometer. The acceleration error thus obtained is used to activate the control surfaces to null the error. Missile attitude rate feedback is required to provide sufficient autopilot loop damping. Acceleration rate, control surface position, and control surface rate are also often used as feedback quantities in system synthesis.

The above description is of a typical high speed aerodynamic vehicle and control system. The unique feature of the system considered in this paper is the control surface actuator. Rather than controlling surface position or surface rate in direct proportion to an actuation signal, this system is controlled by applying full tail (control surface) rate at all times. This fact is expressed by the control equations:

$$\dot{\delta} = +B \qquad m > 0 \tag{1a}$$

$$\dot{\delta} = -B \qquad m < 0 \tag{1b}$$

This method of control gives rise to some special types of behavior which are discussed in the next section.

STABILITY ANALYSIS

Qualitative Discussion

Figure 3 shows a simple diagram of this nonlinear system with a symbolic representation of the actuator. In this system, G(s) and H(s) are such that the autopilot loop is conditionally stable (i.e., a linear actuator coupled with G(s) and H(s) would yield a conditionally stable system). Closing a conditionally stable loop with a bi-stable element such as in this case gives rise to at least two modes of oscillatory operation. These are a low frequency unstable oscillation and a higher frequency stable oscillation. Under most situations, the system will converge to the stable oscillating point.

For manned aircraft, an oscillating autopilot is generally regarded as unacceptable for several reasons. Jitter of the control stick resulting from the oscillation is objectionable to the pilot and wear on the aircraft systems due to continual chatter is undesirable. Missiles, however, have a very short mission time and are nearly always one shot applications so wear and fatigue are not problems.

The higher frequency stable limit cycle oscillation is the mode of operation desired in this control system. A limit cycling state results in an approximately linear characteristic for the actuator for signals which do not exceed the limit cycle amplitude. For small signals then the loop may be analyzed using linear theory and a pseudo-linear gain term for the bi-stable element. The theory of such analyses is well documented by Gorozdos (2) and is not covered in any detail in this report.

It should be noted that for very small amplitude oscillations a linear analysis is of little use since the oscillation is suppressed throughout the major portion of most transients.

Large inputs or disturbances drive the system operating point toward the lower frequency oscillation. If this point is ever reached the system oscillates in a diverging manner with frequency approaching zero and amplitude approaching infinity. Hence, this lower critical frequency is a catastrophic operating point which the system must never be allowed to reach. Unless suitable design precautions are taken, this factor represents a limit on the permissible command level.

For intermediate level inputs which are of most interest from a response point of view, the actuator is not even approximately linear and must be treated as a bang-bang device. When nonlinear control of this type is used, there exists what is called an optimum bang-bang solution or response. If such a response can be achieved, the error in response to a step input is reduced to zero in the minimum possible time. Methods appropriate to this type of solution are applied in a later section to yield the optimum form of the response and the appropriate data for synthesis of an optimum system.

The small signal and stability problems are handled by developing a set of stability surfaces from describing function methods. These surfaces delineate, in a conveniently usable fashion, all the possible points of instability in a three dimensional parameter space. By combining surfaces for various operating regimes, a set of fixed parameters most suitable to the entire flight regime may be selected. These surfaces also

indicate, in a very vivid way, the influence of such factors as airframe stability and actuator parameters on overall system stability.

Stability Criterion and Characteristic Equation

Figure 4 shows a block diagram of the specific control system which is analyzed. In the absence of inputs or initial conditions, a system with a nonlinearity of the type shown in Fig. 4 may exhibit any one of several modes of behavior. To determine the nature of the oscillating modes of operation, it is necessary to apply a suitable stability criterion. For stability analyses of systems with simple nonlinear elements, like the switch under consideration, a describing function is a satisfactory approximation to the true switch characteristic. A switch with output limit B and input sine wave of amplitude a has the describing function:

$$N = 4B/\pi a \tag{2}$$

Notice that the effective gain of the element decreases as the input level increases. This is characteristic of saturating elements, and is of monumental consequence with regard to conditionally stable systems as the discussion to follow will show.

With the nonlinear element represented by its describing function N, the simplest form of the autopilot loop is shown in the following sketch. The approximate characteristic equation for this loop is:

$$1 + NG(s)\,H(s) = 0 \tag{3}$$

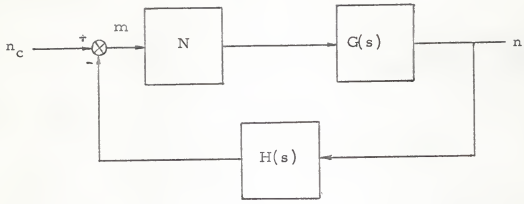

This loop will oscillate at the angular frequency ω_o provided:

$$G(j\omega_o)\, H(j\omega_o) = -1/N \tag{4a}$$

Equation 4a may be equivalently written as:

$$|G(j\omega_o)\, H(j\omega_o)| = 1/N \tag{4b}$$

$$\underline{/G(j\omega_o)\, H(j\omega_o)} = \pm 180^{\circ} \tag{4c}$$

If G(s) and H(s) are specified, then any of the graphical methods of analysis (Bode plots, Nyquist plots, etc.) will suffice to determine the possible frequencies and amplitudes of oscillation. With these methods, however, much effort is required to find a single solution of Eq. (3). One has only experience and past computations as a guide to selecting G(s) and H(s). Considerable trial and error effort is involved in arriving at a design which even then may not be optimum.

An alternate procedure is to solve Eq. (3) explicitly for the points of intersection of $1/N$ and $G(s)\ H(s)$ rather than plotting the two and finding the points graphically. This is accomplished by assuming an oscillation at the frequency ω_o and then solving for the free parameters in $G(s)$ and $H(s)$ necessary to insure this oscillation. These computations are carried out very quickly by machine methods, although hand methods would yield useful data in a reasonable time.

For a steady oscillation to exist at least one pair of roots (a conjugate pair) of the characteristic equation must lie on the imaginary axis. Hence, the necessary condition for an oscillation at the angular frequency ω_o is:

$$1 + NG(j\omega_o)\ H(j\omega_o) = 0 \tag{5}$$

Separating this equation into real and imaginary parts one gets:

$$U(N, \omega_o) + jV(N, \omega_o) = 0 \tag{6}$$

The real and imaginary parts must be zero simultaneously and hence, Eq. (6) provides the two equations:

$$U(N, \omega_o) = 0 \tag{7a}$$

$$V(N, \omega_o) = 0 \tag{7b}$$

These equations could be solved for the frequency of oscillation ω_o and the corresponding N for a particular set of loop parameters. In actual practice, however, the equations are transcendental, and it

is more convenient to write them in the form:

$$U'\left(1/NK_n,\ K_x/K_n\right) = 0 \tag{8a}$$

$$V'\left(1/NK_n,\ K_x/K_n\right) = 0 \tag{8b}$$

By specifying ω_o, these equations may be solved for the pair $(1/NK_n,\ K_x/K_n)$. In this form K_x denotes any one of the feedback gains, and all parameters are normalized with respect to the scale factor K_n. In solving for a specific pair of parameters, all others are held constant. A single solution of Eqs. (8) yields a point $(1/NK_n,\ K_{\dot{n}}/K_n,\ K_{\dot{\theta}}/K_n,\ K_{\ddot{\theta}}/K_n)$ in four space with running parameter ω_o. Later arguments will show that relative values of $K_{\dot{n}}$ and $K_{\dot{\theta}}$ are constrained by the flight regime. Consequently, it is simpler and more convenient to define the ratio

$$K_{\dot{n}}/K_{\dot{\theta}} = K_r \tag{9}$$

and then to use Eqs. (8) to develop a surface in the three space with coordinates $(1/NK_n,\ K_{\dot{\theta}}/K_n,\ K_{\ddot{\theta}}/K_n)$. This surface contains ω_o as a parameter and is developed for a fixed value of K_r.

Derivation of the Stability Equations

To find explicit stability surfaces for the autopilot, it is necessary to derive Eqs.(8). Transfer functions for the airframe under various flight conditions are presented in Appendix A of this paper. The accelerometer and gyro are assumed to be characterized by half critically damped quadratic terms. The control surface actuator is an open loop

device with a pure transportation delay of τ seconds. The block diagram of the composite system showing all of these features is shown in Fig. 5.

Figure 5 is easily reduced to the single loop system of Fig. 6. Distinct parameters for the accelerometer and gyro are used in the derivation of the stability equations to permit study of the influence of various instruments on stability. In general, these instruments have slightly different parameters, although they have been assumed to be alike for the numerical results presented in this paper.

Substituting directly from Fig. 6 into Eq. (3) and simplifying gives:

$$\alpha s^7 + (\beta + \alpha A\bar{K}) s^6 + (\gamma + \beta A\bar{K} - C\alpha) s^5 + \psi + A\bar{K}\gamma - C\beta) s^4$$
$$+(1 + A\bar{K}\psi = C\gamma) s^3 + (A\bar{K} - C\psi) s^2 - Cs + Ne^{-\tau s}\left[K_n DT_g^2 s^s\right.$$
$$+(k_\theta ET_a^2 + K_n DT_g^2 + 2K_n D\zeta_g T_g) s^4 + (K_n D + 2\zeta_a T_a K_\theta E + 2\zeta_g T_g K_n D$$
$$+(K_n \Delta T_g^2 + T_a^2 \{K_\theta E K_\theta \bar{K}\Delta\}) s^3 + (K_\theta E + K_n D + K_n \Delta T_g^2 K_\theta \bar{K}\Delta T_a^2$$
$$+2\zeta_a T_a \{K_\theta E + K_\theta \bar{K}\Delta\} + 2\zeta_g T_g K_n \Delta) s^2 + (\{K_\theta E + K_\theta \bar{K}\Delta + K_n \Delta$$
$$+2\zeta_a T_a K_\theta \bar{K}\Delta \quad 2\zeta_g T_g K_n \Delta) s + (K_n \Delta + K_\theta \bar{K}\Delta) = 0 \qquad (10)$$

The D term defining the normal acceleration per unit of control surface deflection is carried through the literal analysis for generality but is dropped in the numerical analysis because of its small magnitude. Equation (10) is to be solved for $s = j\omega_o$ thus allowing the exponential to be expanded according to the relation:

$$e^{-j\omega_o \tau} = \cos \omega_o \tau - j \sin \omega_o \tau \qquad (11)$$

Substituting $s = j\omega_o$ into Eq. (10), using Eq. (11), and separating into real and imaginary parts gives the following pair of stability equations:

$$\frac{-\alpha\omega_o^7 + (\gamma + \beta A\bar{K} - C\alpha)\omega_o^5 - (1 + A\bar{K}\psi - C\gamma)\omega_o^3 - C\omega_o}{K_n N}$$

$$+ \frac{K_r K_{\dot{\theta}}}{K_n}\left[\mu\left(T_g^2\omega_o^2 - 1\right)\omega_o \cos\omega_o\tau - 2\zeta_g T_g \omega_o^2 \sin\omega_o\tau\right]$$

$$+ \frac{K_{\ddot{\theta}}}{K_n}\left[\left(\bar{K}\Delta - \pi\omega_o^2\right)\omega_o \cos\omega_o\tau - \left(\phi\omega_o^2 - \theta\right)\omega_o^2 \sin\omega_o\tau\right]$$

$$+ \frac{K_{\dot{\theta}}}{K_n}\left[-\left(\phi\omega_o^2 - \theta\right)\omega_o \cos\omega_o\tau + \left(\pi\omega_o^2 - \bar{K}\Delta\right)\sin\omega_o\tau\right]$$

$$- \left[2\mu\zeta_g T_g \omega_o \cos\omega_o\tau \quad \mu\left(T_g^2\omega_o^2 - 1\right)\sin\omega_o\tau\right] = 0 \qquad (12a)$$

$$\frac{-(\beta + \alpha A\bar{K})\omega_o^6 + (\psi + A\bar{K}\gamma - C\beta)\omega_o^4 - (A\bar{K} - C\psi)\omega_o^2}{K_n N}$$

$$+ \frac{K_r K_{\dot{\theta}}}{K_n}\left[2\mu\zeta_g T_g \omega_o^2 \cos\omega_o\tau + \mu\left(T_g^2\omega_o^2 - 1\right)\omega_o \sin\omega_o\tau\right]$$

$$+ \frac{K_{\ddot{\theta}}}{K_n}\left[\left(\phi\omega_o^2 - \theta\right)\omega_o^2 \cos\omega_o\tau + \left(\bar{K}\Delta - \pi\omega_o^2\right)\omega_o \sin\omega_o\tau\right]$$

$$+ \frac{K_{\dot{\theta}}}{K_n}\left[\left(\bar{K}\Delta - \pi\omega_o^2\right)\cos\omega_o\tau - \phi\omega_o^2 - \theta\right)\omega_o \sin\omega_o\tau\right]$$

$$+ \left[\mu\left(T_g^2\omega_o^2 - 1\right)\cos\omega_o\tau - 2\mu\zeta_g T_g \omega_o \sin\omega_o\tau\right] = 0 \qquad (12b)$$

For any parameter set and frequency ω_o which satisfies Eqs. (12), the system will oscillate at the angular frequency ω_o. Further

tests are necessary to determine if the oscillation is stable or unstable. This topic is reserved for discussion at a later point in this paper.

Solution of Stability Equations

Examination of Eqs. (12) shows that upon substitution of a numerical value for ω_o, the equations become algebraic. Note, however, that there are only two equations in three unknowns even if K_r is held constant. A solution is obtained, however, by selecting one parameter (usually $K_{\dot{\theta}}$ or $K_{\ddot{\theta}}$) and solving for values of the remaining pair for all ω_o which have meaning. Obviously, only real positive solutions are of interest. Furthermore, one must exercise care in selecting values of the parameter to be held constant to insure that a solution for the other pair of parameters exists. For machine computations, Eqs. (12) are written in the general form:

$$A_1(\omega_o)/K_n + K_r K_{\dot{\theta}} B_1(\omega_o)/K_n + K_{\dot{\theta}} C_1(\omega_o)/K_n + K_{\ddot{\theta}} D_1(\omega_o)/K_n + E_1(\omega_o) = 0 \tag{13a}$$

$$A_2(\omega_o)/K_n + K_r K_{\dot{\theta}} B_2(\omega_o)/K_n + K_{\dot{\theta}} C_2(\omega_o)/K_n + K_{\ddot{\theta}} D_2(\omega_o)/K_n + E_2(\omega_o) = 0 \tag{13b}$$

where the $A_1(\omega_o)$, $B_1(\omega_o)$, $A_2(\omega_o)$, etc., are algebraic or transcendental functions of ω_o. For specific values of ω_o, these are ordinary algebraic equations which may be solved using Kramer's rule or any other method for simultaneous equations.

Every solution of Eqs. (13) yields a point in three space with coordinates ($1/K_n N$, $K_{\dot{\theta}}/K_n$, $K_{\ddot{\theta}}/K_n$) and with characteristic

frequency ω_o. Repeated solution of Eqs. (13) will thus yield a surface in three space with frequency as a parameter. This surface defines all possible states of oscillation for the given system and thus is a very useful tool in selecting an operating point and in analyzing the system for small inputs. It is now necessary to determine the exact meaning of these surfaces in terms of system operation.

The basic plant and feedback functions of the system under consideration would yield a conditionally stable system if the nonlinear element were replaced with a linear one. Hence, a stable high frequency oscillation and an unstable low frequency oscillation are possible. To investigate the stability of these oscillations, one may consider the nonlinear element as a linear device whose gain decreases with increasing input level (see Eq. (2)). By observing the motion of the roots of the characteristic equation on the s-plane as the oscillation amplitude changes, one may determine the stability of a particular oscillating point. (For purposes of this analysis a stable oscillation is one which has a constant amplitude and frequency and which, when perturbed, returns to this point. An unstable oscillation is one which violates any or all of these conditions.) Consider the root locus sketch of a conditionally stable shown below.

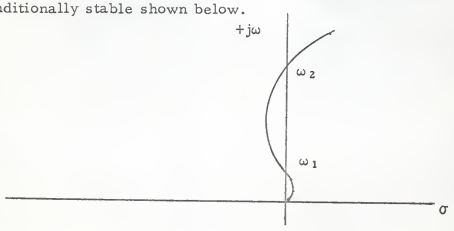

At the higher oscillation frequency ω_2, a positive perturbation in amplitude (which decreases the switch gain), causes the operating point to shift into the left half plane. Here the system is stable and the oscillation tends to die out. This decay in amplitude increases the gain of the nonlinear element and the operating point converges on ω_2 as a stable operating point (an analogous argument to that given above will show that a perturbation into the right half plane at ω_2 will also converge to ω_2).

Very large signals appearing at the switch input cause the operating point to shift from ω_2 toward the origin along the locus. Assume that the switch gain is driven sufficiently low to reach the point ω_1. At this point a slight increase in the switch input (causing a decrease in gain) shifts the operating point into the right half plane. With roots thus in the unstable part of the s-plane, the amplitude of oscillation tends to grow. This further decreases the gain causing the system to diverge with ω_o approaching zero, and the amplitude of oscillation approaching infinity.

A second point should be noted here. As the gain changes with varying signal level, the roots of the characteristic equation move along the root locus. One would thus expect a response which is sensitive to input amplitude. This is indeed the case and this point will be explored later in this paper. Furthermore, from the above discussion, one must beware of inputs which exceed the unsafe boundary at ω_1. The stability surfaces which can be developed from Eqs. (13), delineate the

possible oscillation frequencies (both the stable and unstable ones) and also show in a qualitative sense the permissible disturbance level for stability.

Interpretation of Stability Surfaces

Equations (13) are solved for all values of ω_o which yield real, positive sets of parameters. These data could be presented as a three dimensional plot or surface with coordinates $(1/K_n N,\ K_{\dot{\theta}}/K_n,\ K_{\ddot{\theta}}/K_n)$. With the range of parameters involved, however, it is much more convenient to consider planes taken from the surface at constant values of $K_{\dot{\theta}}$ or $K_{\ddot{\theta}}$ as is illustrated in the sketch below.

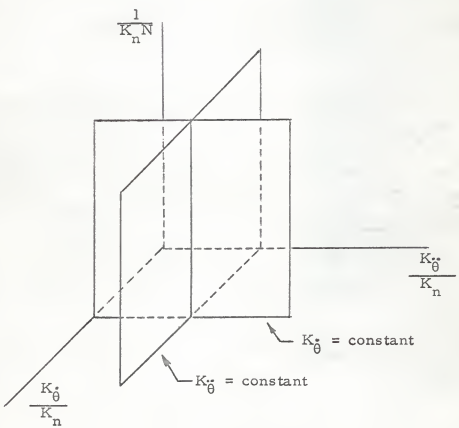

A typical intersection of a plane of constant K_θ and the stability surface is sketched below. The direction of increasing oscillation frequency is indicated by the arrow on the sketch. This result may be interpreted by referring to the root locus sketch for a conditionally stable system also shown on this page. It is true that the root locus method may not be applied directly to a system with a transportation delay.

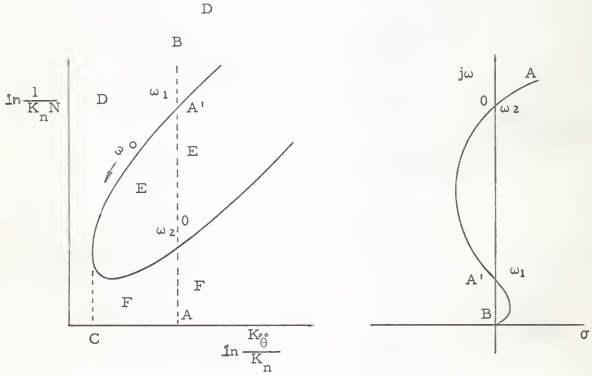

However, the basic form of the stability surfaces is not altered, since the principle influence of the delay is to change slightly the frequency associated with a particular parameter point. Interpretation of the stability boundaries (the two dimensional planes taken from the surface)

in terms of the root locus is thus valid in a qualitative sense although it cannot be used to obtain quantitative data unless the delay is zero.

Returning to the sketches above, operation of the system is restricted to the path A-B on the stability plane and also on the root locus plane. The nonlinear element may be treated as a device whose gain varies inversely with the input amplitude (see Eq. (2)). It has previously been shown that a temporary operating point which lies anywhere between A and A' will eventually become a stable operating point at 0 with frequency ω_2. However, if the system is ever driven to points in the region A'- B, the system will diverge. Referring to the sketches, one sees that decreasing K_{θ} causes more and more of the root locus to lie in the right half plane. When K_{θ} corresponds to point C, the root locus is tangent to the imaginary axis and hence, lies entirely in the right half plane. With these facts in mind, the following interpretations of the areas shown on the stability boundary sketch are obvious:

1. Area D is an unstable region and must be excluded as an operating region. This area may be entered by setting K_{θ} too small ($K_{\theta} < C$) or by subjecting the system to large inputs or disturbances thus traversing the boundary along A-B.

2. Area E is a safe area with some of the instantaneous roots being in the left half plane. Temporary operating points in this region will converge eventually to ω_2 along O-A'.
3. Area F is also a safe area, but the instantaneous roots lie in the right half plane. Temporary points in this area also converge to ω_2 but here along A-0.
4. For $K_{\ddot{\theta}}$ corresponding to point A, the steady state operating point is 0 with oscillation frequency ω_2.

To generate a boundary of the type discussed above, one must, of course, select a value of $K_{\dot{\theta}}$ which yields real, positive $K_{\ddot{\theta}}$. A similar statement applies to boundaries of $K_{\dot{\theta}}$.

Planes of constant $K_{\ddot{\theta}}$ are of the general nature sketched below.

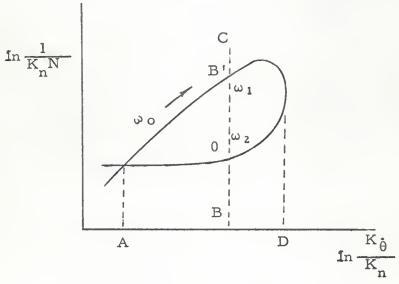

Using arguments similar to those above, one finds that the following interpretations apply to the $K_{\dot{\theta}}$ boundaries.

1. Values of $K_{\dot{\theta}}$ larger than D result in the entire root locus being in the right half plane. Hence, this region must be excluded as an operating region.
2. Any value of $K_{\dot{\theta}}$ between A and D is acceptable with the lower boundary being stable and the upper boundary unstable.
3. For values of $K_{\dot{\theta}}$ less than A, the system, in an undisturbed state, will exhibit a stable high frequency oscillation at ω_2. This linearizes the loop for small signals and hence yields a conditionally stable linear loop. The low frequency gain margin for operation in this region is negative, and the system diverges. This divergence is characterized by a constant amplitude oscillation at ω_2 with a superimposed low frequency oscillation with amplitude approaching infinity and frequency approaching zero.

Planes of constant $1/N$ do not contribute any additional information.

Numerical Results

Two flight regimes, representing a typical range on q^*, have been selected for study. In addition, an extreme range of airframe stability, associated with various center of gravity locations, is considered for the high q flight condition. These combinations are sufficient to illustrate the use of the method of analysis and the range of parameters to be expected. Table 1-A lists aerodynamic parameters for the conditions considered.

Table 1-A. Aerodynamic parameters used in calculating stability data.

A	D	C	E	$\bar{K}$	Flight condition number
1.00	0	0	229.0	1.1	1
1.00	0	-100	229.0	1.1	2
1.00	0	100	229.0	1.1	3
1.00	0	0	229.0	0	4
.116	0	0	26.0	1.7	5
.116	0	0	26.0	0	6

Table 1-B lists, for the aerodynamic parameters listed in Table 1-A, the feedback parameters for which stability data have been obtained. The resulting data are presented in the figures listed in the table and are discussed below.

* See page 43 for nomenclature.

Table 1-B. Feedback and actuator parameters used in calculating stability data.

Flight condition	$K_{\dot{\theta}}$			$K_{\ddot{\theta}}$			τ	Fig. No.
1	0.1	0.03	0.01				0.01	7
5	0.1	0.03	0.01				0.01	8
1				0.03	0.01	0.003	0.01	9
5				0.01	0.003	0.001	0.01	10
1, 2, 3		0.03					0.01	11
1, 2, 3					0.003		0.01	12
1		0.03					0.01	13
1					0.003		0.01	14

Figures 7 and 8 show $K_{\ddot{\theta}}$ boundaries for high q and low q conditions, respectively. Similarly, Figs. 9 and 10 are $K_{\dot{\theta}}$ boundaries for high and low q conditions. The boundaries associated with the different q levels are not radically different, however, it should be noted that the high q condition generally dictates the values of $K_{\dot{\theta}}$ and $K_{\ddot{\theta}}$. The actual values of $K_{\dot{\theta}}$ and $K_{\ddot{\theta}}$ are selected based on relative stability, small signal response, and to some extent, the time domain analysis presented later in this paper.

Data for flight conditions 1, 2, and 3 are presented in Figs. 11 and 12. These data show that airframe stability influences the upper portion of the loop stability boundary and hence the disturbance level at which the system may be expected to diverge. From Fig. 11, one sees that a very stable airframe results in an autopilot which cannot be driven unstable whereas an unstable airframe aggravates the disturbed stability problem causing the autopilot to diverge for very small inputs.

Figures 13 and 14 illustrate the influence of actuator delay on the stability boundaries and hence on the stability of the overall system. As can be readily seen, the safe operating area decreases rapidly as τ increases. Also, the frequencies on the acceptable operating region of the boundary are much lower for large τ. Lower frequencies result in larger chatter amplitudes, and consequently more wear and tear on the system hardware. Small horsepower actuators with delays of 0.01 seconds are in existence but any appreciable reduction in this figure will be difficult.

SMALL SIGNAL ANALYSIS

The steady state mode of operation for the system under analysis is a high frequency limit cycle. This limit cycle linearizes the nonlinear element so that a linear analysis may be carried out by assigning a pseudo-linear gain term to the switch. Such an analysis is valid only so long as the limit cycle is not interrupted during any portion of the response.

In developing the stability surfaces, the describing function or gain at the oscillation frequency of the nonlinear element is taken as N. It can be shown (2) that the effective gain of the switch for small control signals is just N/2.

$$K_N = N/2 \tag{14}$$

With this simple relation, one may determine the gain appropriate for a linear small signal analysis directly from the

the stability surface. With a pseudo-linear gain for the switch thus established, conventional linear theory will yield the response of the autopilot for small signals.

TIME DOMAIN ANALYSIS

Switch Characteristic

The preceding parts of this paper have shown a method for the steady state analysis of the nonlinear autopilot being discussed. Further, the small signal response of the system can be determined from this analysis coupled with conventional linear theory. Large signals, however, interrupt the oscillation and linear theory no longer suffices to determine the system response.

With the loop operating in a steady limit cycle, the switch may be characterized as sketched below. The smaller linear portion of the characteristic results from the limit cycle linearization of the switch. For most cases, the linear region is so small relative to m, that the switch characteristic may be taken as that of an ideal, infinite gain limiter.

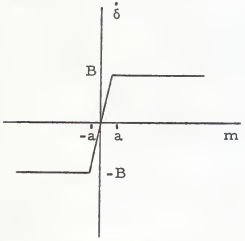

Actual Characteristic

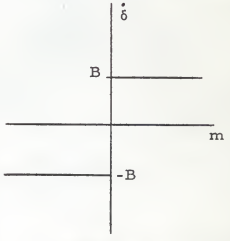

Approximate Characteristic

Optimum Response

For a bang-bang or switch type controller, there exists an optimum response to an input or disturbance. Such a response reduces the error to zero in a minimum possible time. It can be shown that this optimum response occurs when the two rules below for switching the limited variable are satisfied.

1. The limited variable is at its maximum absolute value throughout the response.
2. The limited variable changes sign $(n-1)$ times where n is the number of poles.

According to Schmidt, (4), these rules were derived for a plant with real poles but are applicable to systems with complex poles provided the damping is not extremely light.

From the definition of optimum response, the error and $n-1$ of its derivatives must be zero at T_m, the response or solution time. Note that for step inputs the error derivatives are the feedback quantity derivatives. Thus the optimum response parameters (the reversal times T_1, and T_2, and the response time T_m) may be found by writing the error and error derivative equations and solving them simultaneously. This method, of course, depends on rules 1 and 2 to determine these error equations.

A much more elegant and direct method of finding the optimum response parameters is to use rules 1 and 2 and the theory of Laplace transforms. To this end, consider the simple control loop shown in the sketch.

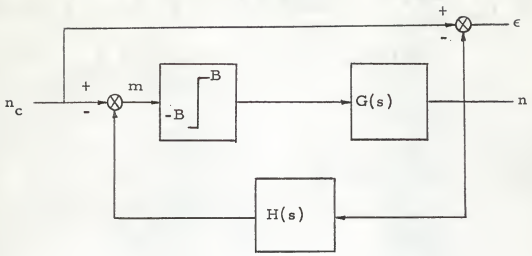

Assuming that the input n_c is a unit step at $t = 0$, and that the system is designed to give optimum response, then the error $\epsilon(t)$ obeys the conditions:

$$\epsilon(t) = 0 \qquad t < 0 \tag{15a}$$

$$\epsilon(t) = 0 \qquad t > T_m \tag{15b}$$

Now $\epsilon(t)$ is a truncated time signal (i.e., zero for all but a finite time interval) and must, according to the theory of Laplace transforms, have a transform which is an entire function. Using rules 1 and 2 and the sketch, one may write the Laplace transform of the system error. Forcing this function to be entire yields the optimum switching parameters.

An analysis of the type outlined above yields the optimum switching or reversal times and the optimum response times. Armed with these data, it is a simple matter to calculate the actual response as well as the error and its derivatives during the transient portion of the response. Furthermore, one may use these data

to synthesize an optimum system.

Optimum Control System for a Simple Airframe

Derivation of Switch Time Equations. To a first approximation the airframe transfer function* is

$$\frac{n}{\dot{\delta}} = \frac{AE}{s^3} \tag{16}$$

Using this approximation of the airframe and the methods outlined, an optimum system design will be consumated.

Since the plant is third order, rule 2 requires two switch reversals. From this and rule 1, the optimum form of switching is that shown in the sketch below.

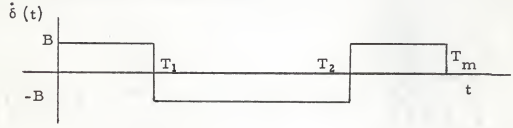

Using delay functions, $\dot{\delta}(t)$ is written in terms of the unknown switch times as

$$\dot{\delta}(t) = B\left[1 - 2u(t - T_1) + 2u(t - T_2) - u(t - T_m)\right] \tag{17}$$

which has Laplace transform

$$\dot{\delta}(s) = \frac{B}{S}\left[1 - 2e^{-T_1 S} + 2e^{-T_2 S} - e^{-T_m S}\right] \tag{18}$$

On the next page is shown that portion of the system associated

* This representation has often been used in actual system analysis but is, of course, of restricted accuracy.

with the analysis to follow.

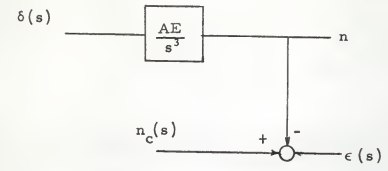

From this sketch one writes

$$\epsilon(s) = n_c(s) - n(s) \tag{19a}$$

$$= n_c(s) - \frac{AE}{s^3}\,\dot{\delta}\,(s) \tag{19b}$$

$$= \frac{n_c}{s} - \frac{BAE}{s^4}\left[1 - 2e^{-T_1 s} + 2e^{-T_2 s} - e^{-T_m s}\right] \tag{19c}$$

where the latter form of the equation assumes that n_c is a step. According to Schmidt (4) the optimum solution is given if Eq. (19c) is such that there are no poles in the finite s-plane. This condition is satisfied provided:

$$T_1 = \left(\frac{n_c}{2ABE}\right)^{1/3} \tag{20a}$$

$$T_2 = 3T_1 \tag{20b}$$

$$T_m = 4T_1 = 4\left(\frac{n_c}{2ABE}\right)^{1/3} \tag{20c}$$

From these equations note the following pertinent items:

1. The response time varies with n_c such that an 8g maneuver takes twice as long as a 1g maneuver.

2. Since A and E are each proportional to q, the response time varies as $q^{-2/3}$. Thus it takes considerably longer to pull a 2g manuever at 50,000 feet altitude than it does at sealevel.
3. The response time decreases as the control surface rate limit is increased. However, actuator power consumption and chatter amplitude both vary linearly with this rate limit.
4. The switching is symmetrical and thus the control surface rate is negative for the same length of time as it is positive. Thus, of course, the final tail position is the same as the initial position.

It should also be noted that although the response time varies with q and n_c, this is usually acceptable from a guidance system point of view provided certain bounds are observed.

Synthesis of Optimum System. The feedback quantities in this system are n, $\dot{n}$, $\dot{\theta}$, $\ddot{\theta}$, These may be written (at the switch times) as:

$$n(T_1) = \frac{BAE}{6} T_1^3 = \frac{n_c}{12} \tag{21a}$$

$$\dot{n}(T_1) = \frac{BAE}{2} T_1^2 \sim B^{1/3} q^{2/3} n_c^{2/3} \tag{21b}$$

$$\dot{\theta}(T_1) = \frac{BE}{2} T_1^2 \sim B^{1/3} q^{-1/3} n_c^{2/3} \tag{21c}$$

$$\ddot{\theta}(T_1) = BE\ T_1 \sim B^{2/3} q^{1/3} n_c^{1/3} \tag{21d}$$

From symmetry of optimum switching:

$$n(T_2) = 11n_c/12 \tag{22a}$$

$$\dot{n}(T_2) = \dot{n}(T_1) \tag{22b}$$

$$\dot{\theta}(T_2) = \dot{\theta}(T_1) \tag{22c}$$

$$\ddot{\theta}(T_2) = -\ddot{\theta}(T_1) \tag{22d}$$

At the end of the response:

$$t = T_m$$

$$n = n_c$$

$$\dot{\theta} = \ddot{\theta} = \dot{n} = \dot{\delta} = 0$$

Expressions for the feedback quantities, assuming an optimum response, are given by Eqs. (21) and Eqs. (22). These data must now be used to select $K_{\dot{\theta}}$, $K_{\ddot{\theta}}$, $K_{\dot{n}}$, and K_n, such that optimum switching actually occurs. The optimum switching criteria are simply constraints on the actuating signal given as:

$$m(T_1) = 0 \tag{23a}$$

$$m(T_2) = 0 \tag{23b}$$

$$\frac{\partial m(T_1)}{\partial t} < 0 \qquad \frac{\partial m(T_2)}{\partial t} > 0$$

The partial derivatives which insure proper direction of switching were considered in writing the equation for $\dot{\delta}(t)$ and hence, are automatically satisfied. From Fig. 15, the general form of the actuating signal is:

$$m(t) = n_c(t) - K_n\, n(t) - K_{\dot{\theta}}\, \dot{\theta}(t) - K_{\ddot{\theta}}\, \ddot{\theta}(t) - K_{\dot{n}}\, \dot{n}(t) \tag{24}$$

Substituting Eqs. (21) and Eqs. (22) into Eq. (24) gives, respectively:

$$m(T_1) = 0 = \frac{11n_c}{12} - K_r K_{\dot{\theta}}^{\cdot} R_1 n_c^{2/3} - K_{\ddot{\theta}}^{\cdot\cdot} R_3 n_c^{1/3} - K_{\dot{\theta}}^{\cdot} R_2 n_c^{2/3} \tag{25a}$$

$$m(T_2) = 0 = \frac{n_c}{12} - K_r K_{\dot{\theta}}^{\cdot} R_1 n_c^{2/3} - K_{\dot{\theta}}^{\cdot} R_2 n_c^{2/3} + K_{\theta} R_3 n_c^{1/3} \tag{25b}$$

In these equations, $K_n = 1$ and the R's are functions of A, B, and E, and are constants for a given flight condition. The definition $K_n^{\cdot} = K_r K_{\theta}$ is also used in these equations.

Inspection of Eqs. (25) shows that n_c appears to various powers in the terms of the equations. Thus these equations cannot be satisfied for all n_c with constant values for the feedback gains. If, instead of linear gains, one uses the cube root of the error and the square root of the rate feedback terms, the n_c terms in the equations may be divided out. Rewriting Eqs. (25) in the form

$$m(T_1) = 0 = \frac{11n_c}{12} - K_{\dot{\theta}}^{\cdot} (K_r R_1 + R_2) n_c^{2/3} - K_{\ddot{\theta}}^{\cdot\cdot} R_3 n_c^{1/3} \tag{26a}$$

$$m(T_2) = 0 = \frac{n_c}{12} - K_{\dot{\theta}}^{\cdot} (K_r R_1 + R_2) n_c^{2/3} + K_{\theta} R_3 n_c^{1/3} \tag{26b}$$

and using the suggested non-linear gains gives

$$m(T_1) = 0 = \left(\frac{11n_c}{12}\right)^{1/3} - K_{\dot{\theta}}^{\cdot} \sqrt{K_r R_1 + R_2}\, n_c^{1/3} - K_{\ddot{\theta}}^{\cdot\cdot} R_3 n_c^{1/3} \tag{27a}$$

$$m(T_2) = 0 = \left(\frac{n_c}{12}\right)^{1/3} - K_{\dot{\theta}}^{\cdot} \sqrt{k_r R_1 + R_2}\, n_c^{1/3} + K_{\ddot{\theta}}^{\cdot\cdot} R_3 n_c^{1/3} \tag{27b}$$

These equations no longer involve n_c and may be solved simultaneously for $K_{\dot{\theta}}^{\cdot}$ and $K_{\ddot{\theta}}^{\cdot\cdot}$. These values would then yield

a system which is optimum for all n_c. Note, however, that the equations still contain the aerodynamic parameter q and, hence, the above optimum solution is valid only at the particular q for which the solution was taken.

An approximation to the q variation can be made by taking appropriate combinations of the feedback parameter pair $\dot{\theta}$ and $\dot{n}$ and of the pair δ and $\ddot{\theta}$. The use of δ feedback was not considered in the frequency domain analysis presented earlier, so only an indication of the results in the time domain will be given here.

Referring to Eq. (26a), the coefficient of the $K_{\dot{\theta}}$ term is

$$K_r R_1 + R_2$$

which in terms of q becomes

$$K_r q^{2/3} + q^{-1/3}$$

where the constant multiplier has been discarded. It is desired to make this term as near q independent as possible using the simple relation above (a polynomial in q could be introduced at the expense of great complication of the hardware). The parameter K_r is selected by equating the above term for two different values of q and solving for K_r. Thus

$$K_r\, q_1^{2/3} + q_1^{-1/3} = q_2^{-1/3} + K_r\, q_2^{1/3} \tag{28}$$

for a reasonable set of q_1 and q_2 (although not necessarily optimum) one finds $K_r = 1.5$, is satisfactory. Using an approach

similar to that above, one finds that a suitable ratio, K_L of δ feedback to $\ddot{\theta}$ feedback is .03.

Analog Data for Optimum System. Actual response traces, taken from an analog simulation of the above system, are shown in Figs. 15 and 16. For this simulation, diode function generators were used to approximate the nonlinear functions. The analog computer traces, on which is shown the theoretical optimum response times, demonstrate the validity of the above approach.

The above system has adequate response over a large q range without the use of air data scheduling. Furthermore, the system is faster than a normal linear system designed around a comparable airframe. Introduction of the nonlinear gain terms precludes the possibility of driving the system unstable with large inputs.

An important feature of an optimum response is the absence of overshoot without the consequent long response time associated with overdamped linear systems. This feature is evident in Figs. 16 and 17.

Switch Time Equations for Neutrally Stable Airframe

The preceding discussion has considered a simple approximation to the actual airframe. Despite the approximation, switch time data obtained from this analysis are in surprisingly good agreement with the results of more accurate analyses.

Almost every missile airframe has, at some point in the flight regime, a condition of neutral stability. This simply implies that a

perturbation in the angle of attack causes no restoring moment to correct for the disturbance. From a control point of view, a neutrally stable airframe is desirable since such an airframe is easy to control and at the same time does not unduly aggravate the loop stability problem. It is never possible, however, to maintain a given degree of airframe stability over the entire flight regime. Consequently, it is necessary that the autopilot loop be designed to cope with a range of values of the airframe stability parameter C. The two most important cases $C = 0$, and $C > 0$ are considered below.

A neutrally stable airframe has transfer function:

$$\frac{n}{\dot{\delta}} = \frac{AE}{s^2(s + A\bar{K})} \tag{29}$$

Since this is a third order plant, the equation for $\delta(s)$ is:

$$\dot{\delta}(s) = \frac{B}{s}\left[1 - 2e^{-T_1 s} + 2e^{-T_2 s} - e^{-T_m s}\right] \tag{30}$$

Using Eqs. (18) and (19), the error transform can be written as:

$$\epsilon(s) \quad \frac{n_c}{s} - \frac{BAE\left[1 - 2e^{-T_1 s} + 2e^{-T_2 s} - e^{-T_m s}\right]}{s^3(s + A\bar{K})} \tag{31}$$

This function has no poles in the finite s-plane if:

$$0 = 2T_1 - 2T_2 + T_m \tag{32a}$$

$$0 = 1 - 2e^{A\bar{K}T_1} + 2e^{A\bar{K}T_2} - e^{A\bar{K}T_m} \tag{32b}$$

$$\frac{n_c \bar{K}}{BE} = T_2^2 - T_1^2 - \frac{T_m^2}{2} \tag{32c}$$

Useful literal expressions for T_1, T_2, and T_m cannot be

obtained from these equations necessitating a numerical machine method of solution.

Switch Time Equations for Unstable Airframe

An unstable airframe is defined by $C > 0$ and may be caused by center of gravity shifts with changing fuel load, center of pressure shifts or any number of other causes. It was previously shown that an unstable airframe results in a control loop which diverges for much smaller inputs or distrubances. A rather surprising result of the analysis to follow is that the response time for the loop with $C > 0$ is actually longer than for the $C = 0$ case.

With $C > 0$ the airframe transfer is

$$\frac{n}{\delta} = \frac{AE}{s(s^2 + A\bar{K}s - C)} = \frac{AE}{s(s + a_1)(s + a_2)} \tag{33}$$

where

$$a_1 = \frac{A\bar{K} + \sqrt{(A\bar{K})^2 + 4C}}{2} \qquad a_1 > 0 \tag{34a}$$

$$a_2 = \frac{A\bar{K} - \sqrt{(A\bar{K})^2 + 4C}}{2} \qquad a_2 < 0 \tag{34b}$$

The error transform for this case is

$$\epsilon(s) = \frac{n_c}{s} \quad \frac{-BAE}{s^2(s + a_1)(s + a_2)} \left[1 - 2e^{-T_1 s} + 2e^{-T_2 s} - e^{-T_m s} \right] \tag{35}$$

For optimum switching, one gets:

$$0 = 1 - 2e^{a_1 T_1} + 2e^{a_1 T_2} - e^{a_1 T_m} \tag{36a}$$

$$0 = 1 - 2e^{a_2 T_1} + 2e^{a_2 T_2} - e^{a_2 T_m} \tag{36b}$$

$$\frac{n_c C}{BAE} = 2T_2 - 2T_1 - T_m \tag{36c}$$

Solution of these equations was also carried out using machine computation.

Optimum Switch Time Data

Optimum switch time data for the flight conditions in Table 2 are presented in Figs. 18 through 21.

Table 2. Aerodynamic parameters used in finding optimum switch time data.

Flight condition	A	D	E	$\bar{K}$	Control Surface Rate Limit B
1	1.0	0	229.0	1.1	200
8	1.0	49.0	229.0	1.1	200
4	1.0	0	229.0	0	200
5	0.116	0	26.0	1.7	200
7	0.116	5.53	26.0	1.7	200
6	0.116	0	26.0	0	200

These figures illustrate the small differences in switch times associated with the various airframes. As would be expected, the unstable airframe requires the first switch point to occur early, otherwise, the angle of attack would get uncontrollably large. The rather unexpected result, however, is the longer response time associated with the

unstable airframe.

Synthesis Procedure

With the simple airframe considered earlier, it was fairly easy to write literal expressions for the switching times and switching equations. The more exact airframe representation, however, requires the use of numerical methods as outlined below.

As before, the switching criteria are

$$m(T_1) = 0 \tag{37a}$$

$$m(T_2) = 0 \tag{37b}$$

$$\frac{\partial\, m(T_1)}{\partial\, t} < 0, \quad \frac{\partial\, m(T_2)}{\partial\, t} > 0$$

provided there is no delay time. To achieve optimum response, the limited variable $\dot{\delta}$ must actually change sign at T_1 and T_2. If the actuator has delay, then the actuating signal must anticipate the reversals by τ seconds. Hence, the switching criteria in the presence of delay become:

$$m(T_1 - \tau) = 0 \tag{38a}$$

$$m(T_2 - \tau) = 0 \tag{38b}$$

$$\frac{\partial\, m(T_1 - \tau)}{\partial\, t} < 0 \quad \frac{\partial\, m(T_2 - \tau)}{\partial\, t} > 0$$

The partial derivatives are satisfied by the expression for $\dot{\delta}(s)$

and the other constraints may be written as:

$$m(T_1 - \tau) = 0 = n_c - K_n n(T_1 - \tau) - K_r K_{\dot{\theta}} \dot{n}(T_1 - \tau) - K_{\dot{\theta}} \dot{\theta}(T_1 - \tau) - K_{\ddot{\theta}} \ddot{\theta}(T_1 - \tau) \tag{39a}$$

$$m(T_2 - \tau) = 0 = n_c - K_n n(T_2 - \tau) - K_r K_{\dot{\theta}} \dot{n}(T_2 - \tau) - K_{\dot{\theta}} \dot{\theta}(T_2 - \tau) - K_{\ddot{\theta}} \ddot{\theta}(T_2 - \tau) \tag{39b}$$

The feedback quantities may easily be found from the equations:

$$n(t) = L^{-1}\left[\dot{\delta}(s)\, G(s)\right] \tag{40a}$$

$$\dot{n}(t) = \frac{d}{dt}\, n(t) \tag{40b}$$

$$\dot{\theta}(t) = n(t)\, \overline{K} + \frac{\dot{n}(t)}{A} \tag{40c}$$

$$\ddot{\theta}(t) = E\, \delta(t) + C\, \frac{n(t)}{A} \tag{40d}$$

$$\delta(t) = B\left[t - (t - T_1)\, u(t - T_1) + (t - T_2)\, u(t - T_2)\right]$$

With K_r and K_n specified, Eqs. (39) may be solved simultaneously for the optimum values of $K_{\dot{\theta}}$ and $K_{\ddot{\theta}}$. To this end, a digital computer program was prepared to yield:

1. The optimum switch times for $C = 0$ and $C > 0$.
2. The solutions of Eqs. (40) and (41) at $t = T_1 - \tau$ and $t = T_2 - \tau$.
3. The simultaneous solution of Eqs. (39) for optimum values of $K_{\dot{\theta}}$ and $K_{\ddot{\theta}}$.
4. The computation and plotting of $n(t)$ from Eq. (40a).

Figure 22 shows the values of $K_{\dot{\theta}}$, as determined from Eqs. (39), plotted versus the command acceleration n_c. Data are shown

for the two extreme flight conditions. Notice that the optimum $K_{\dot{\theta}}$ values for the low q condition are very nearly equal to those for the high q case. This is due directly to the use of $\dot{n}$ feedback (which introduces the parameter K_r) in combination with $\dot{\theta}$ feedback to render $K_{\dot{\theta}}$ independent of q. The results shown in Fig. 21 indicate that 1.5 is a good choice for K_r.

The optimum gain data shown in Figs. 22 and 23 are strong functions of n_c. To remove this dependence, at least two nonlinear gain functions must be introduced. To find appropriate functions for these gains, one must apply numerical methods to the data obtained from Eqs. (39) and Eqs. (40). This operation was not carried out since the data obtained are valid only for a specific set of airframe parameters and are thus of little general use. Results obtained analytically for the simple airframe indicate the general nature of these nonlinear gains. In selecting nonlinear gains, it should be noted that the small signal values are determined by the frequency domain stability analysis.

ACKNOWLEDGMENT

The author wishes to express appreciation to Dr. R. G. Nevins, major professor, for his help in preparing the manuscript, and to Gordon Trotter of the Applied Physics Laboratory, Johns Hopkins University, for his help in preparing the digital computer programs. Appreciation is also expressed to the Applied Physics Laboratory for the use of their analog computer equipment.

REFERENCES

1. Alex, Frederic R. and C. R. Heerman
A study of Russian feedback control theory. WADD Technical Report 61-32, Part I.

2. Gorozdos, R. E.
Frequency analysis of a control loop containing a bistable element. APL/JHU Report CF-2750.

3. Kuo, Benjamin C.
Automatic control systems. Englewood Cliffs: Prentice-Hall, 1962.

4. Schmidt, Stanley F.
The analysis and design of continuous and sampled-data feedback control systems with a saturation type nonlinearity. NASA TN-D20.

5. Schmidt, Stanley F. and Eleanor V. Harper
The design of feedback control systems containing a saturation type nonlinearity. NASA TN-D324.

NOMENCLATURE

$\dot{\delta}$	control surface rate
B	control surface rate limit
m(t)	actuation signal
G(s)	forward path transfer function
H(s)	feedback path transfer function
q =	$1/2\ kpM^2$ dynamic pressure
N	describing function of non-linear element
a	sine wave amplitude at input to non-linear element
ω_o	angular oscillation frequency
$U(N_1, \omega_o$	real part of characteristic equation
$V(N_1, \omega_o)$	imaginary part of characteristic equation
K_n	acceleration feedback gain
$K_{\dot{n}}$	acceleration rate feedback gain
$K_{\dot{\theta}}$	body angular rate feedback gain
$K_{\ddot{\theta}}$	body angular acceleration feedback gain
K_r	$K_{\dot{n}} / K_{\dot{\theta}}$
A	g's per degree angle of attack
D	g's per degree control surface incidence
C	body angular acceleration per degree angle of attack
E	body angular acceleration per degree control surface incidence
$\overline{K}$	angle of attack rate due to lateral acceleration
τ	actuator delay time
Δ	AE - DC

NOMENCLATURE concl.

$\omega_{na} = \frac{1}{T_a}$ accelerometer natural frequency

$\omega_{ng} = \frac{1}{T_g}$ gyro natural frequency

ζ_a accelerometer damping ratio

ζ_g gyro damping ratio

n_c command acceleration

δ control surface incidence

ω_2 high frequency oscillation frequency

ω_1 low frequency oscillation frequency

K_N gain of the non-linear element for small signals

ϵ system error

T_1 first reversal time of optimum response

T_2 second reversal time of optimum response

T_m optimum response time

$\alpha = T_a^2 T_g^2$

$\beta = 2\zeta_a T_a T_g^2 + 2\zeta_g T_g T_a^2$

$\gamma = T_a^2 + T_g^2 + 4\zeta_a T_a \zeta_g T_g$

$\psi = 2\zeta_a T_a + 2\zeta_g T_g$

$\theta = 2\bar{K}\Delta\zeta_a T_a + E$

$\pi = \bar{K}\Delta T_a^2 + 2\zeta_a T_a E$

$\phi = E T_a^2$

$\mu = 2\zeta_g T_g$

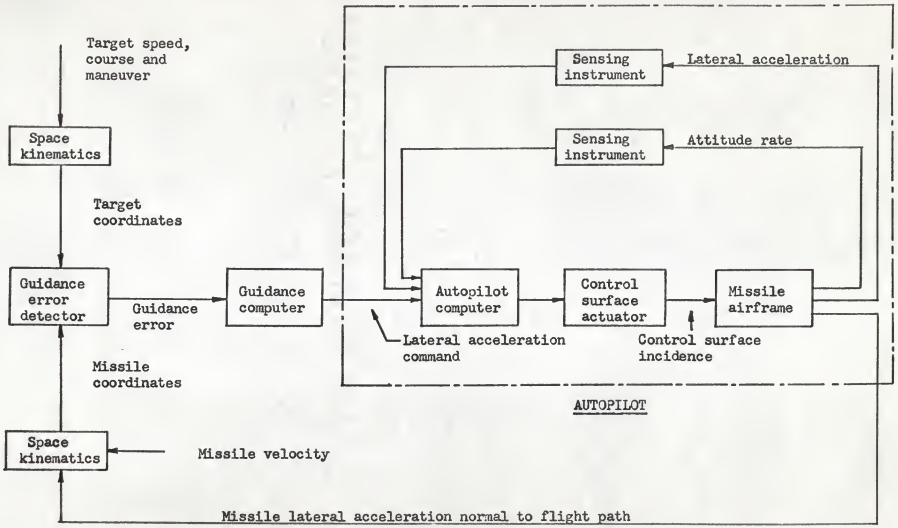

Fig. 1 Typical guided missile functional block diagram.

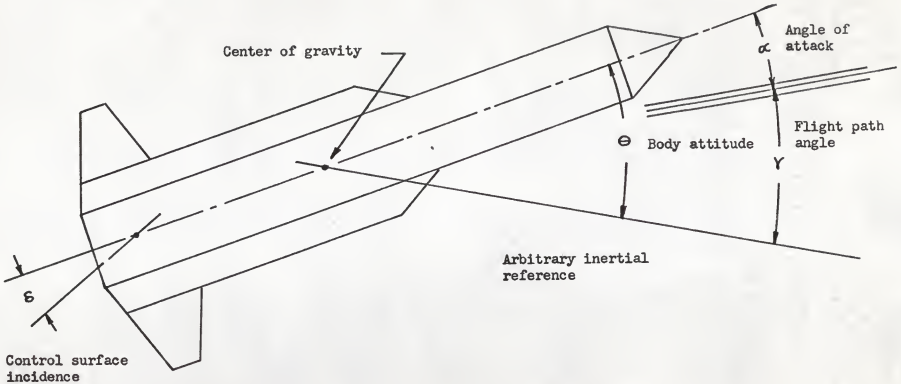

Fig. 2 Pitch plane nomenclature.

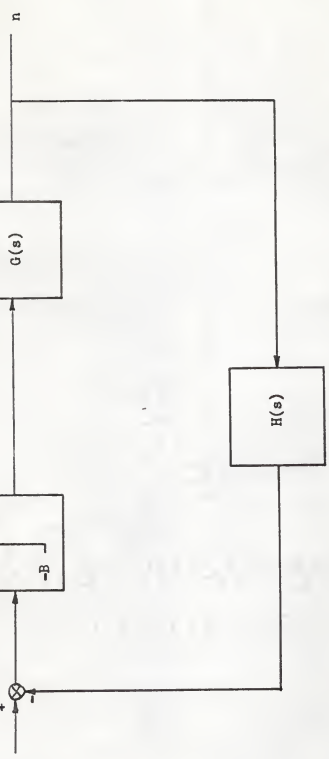

Fig. 3 Simple block diagram illustrating nonlinear element.

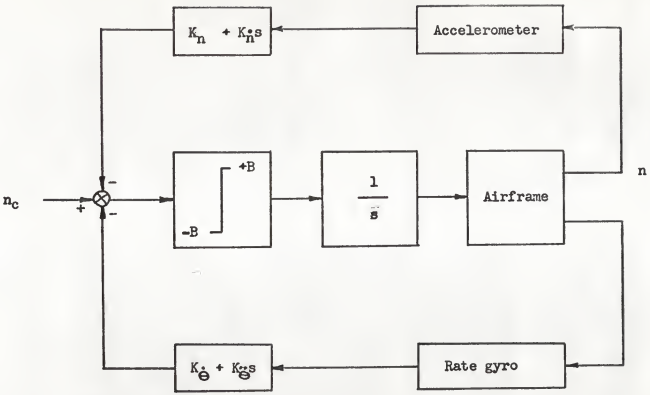

Fig. 4 Nonlinear autopilot block diagram.

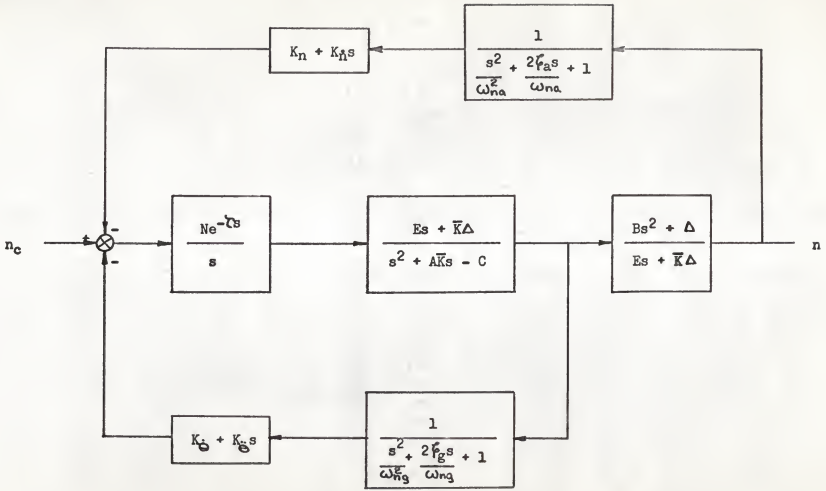

Fig. 5 Autopilot transfer function block diagram.

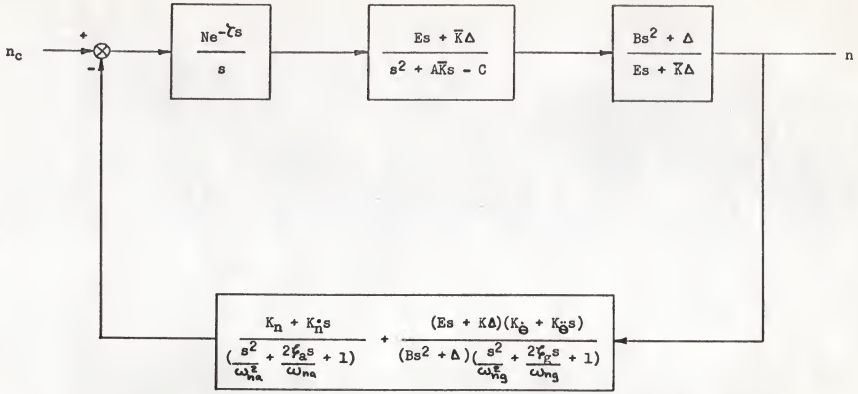

Fig. 6 Autopilot reduced to single loop system.

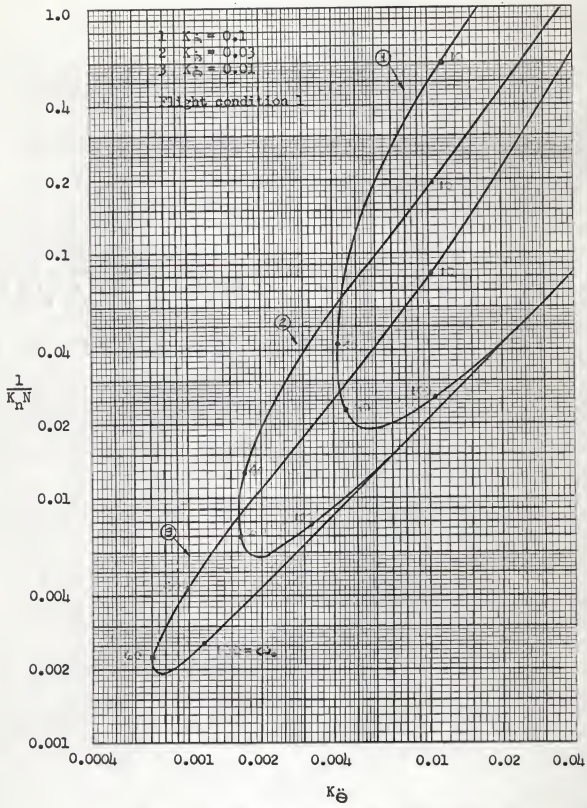

Fig. 7 $K_{\ddot{\theta}}$ stability boundaries for various $K_{\dot{\theta}}$ at high q condition.

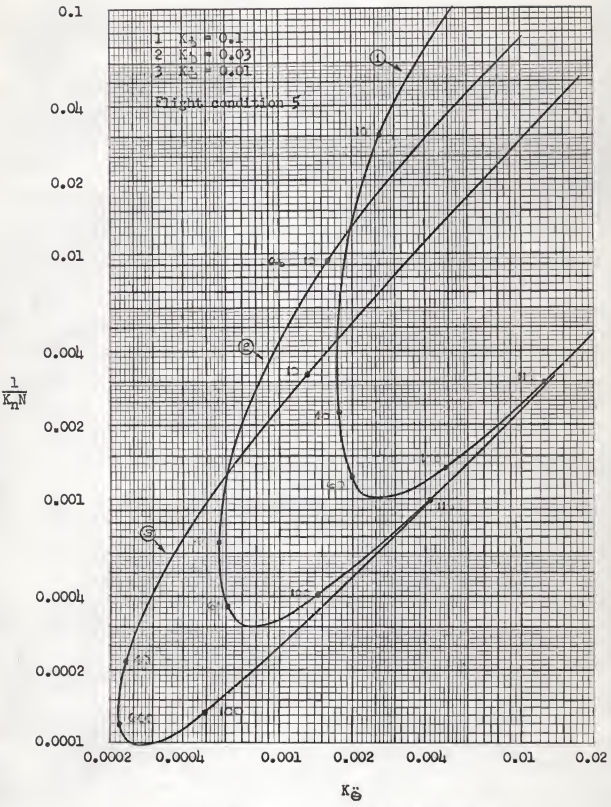

Fig. 8 $K_{\dot{\theta}}$ stability boundaries for various $K_{\dot{\theta}}$ at low q condition.

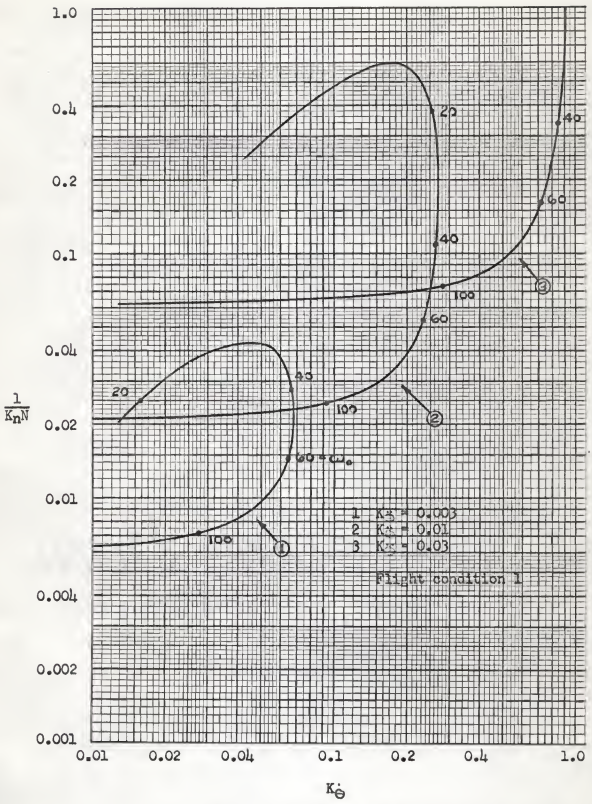

Fig. 9 $K_{\dot{\theta}}$ stability boundaries for various $K_{\ddot{\theta}}$ at high q flight condition.

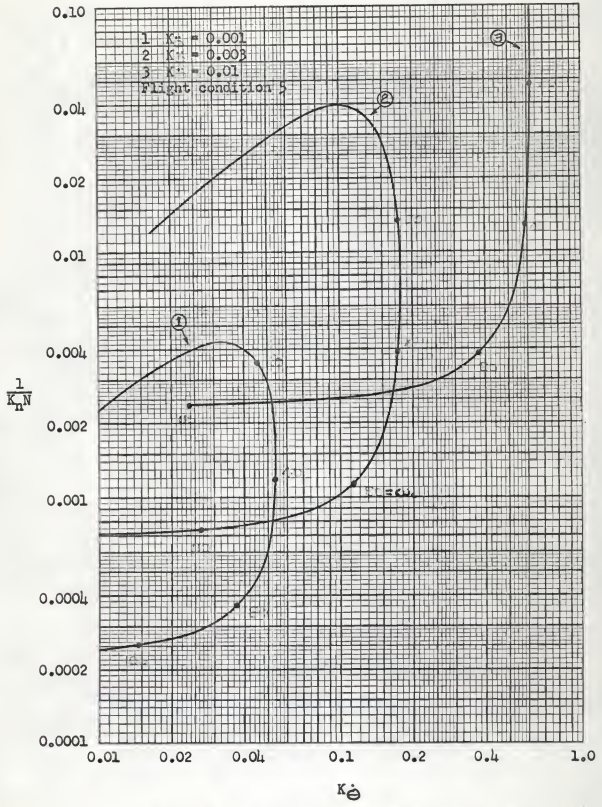

Fig. 10 K$\dot{\theta}$ stability boundaries for various K$\dot{\theta}$ at a low q flight condition.

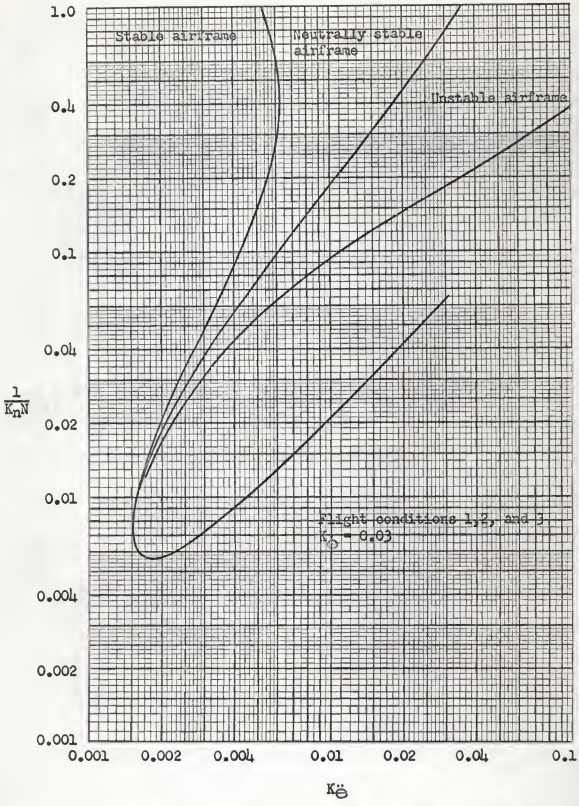

Fig. 11 $K_{\dot{\theta}}$ stability boundary illustrating influence of airframe stability on system stability.

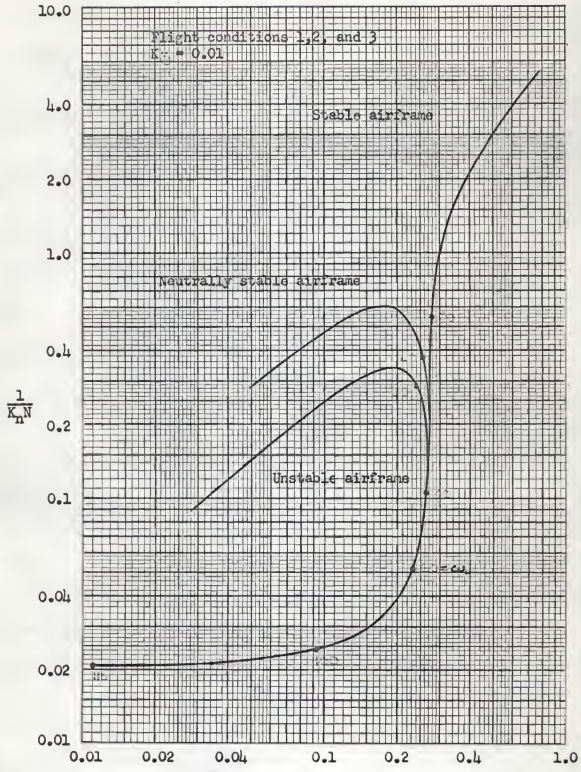

Fig. 12 $K_{\dot{\theta}}$ stability boundary illustrating influence of airframe stability on system stability.

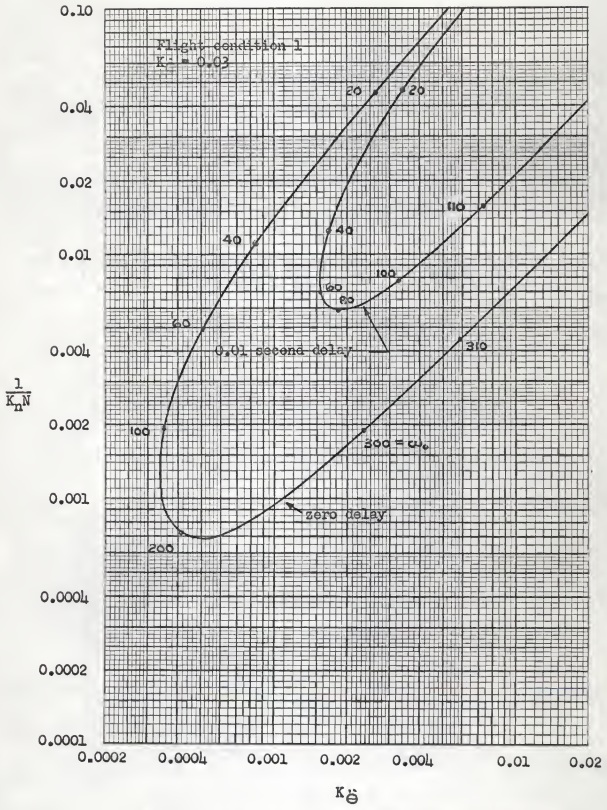

Fig. 13 Stability boundary illustrating influence of actuator delay on system stability.

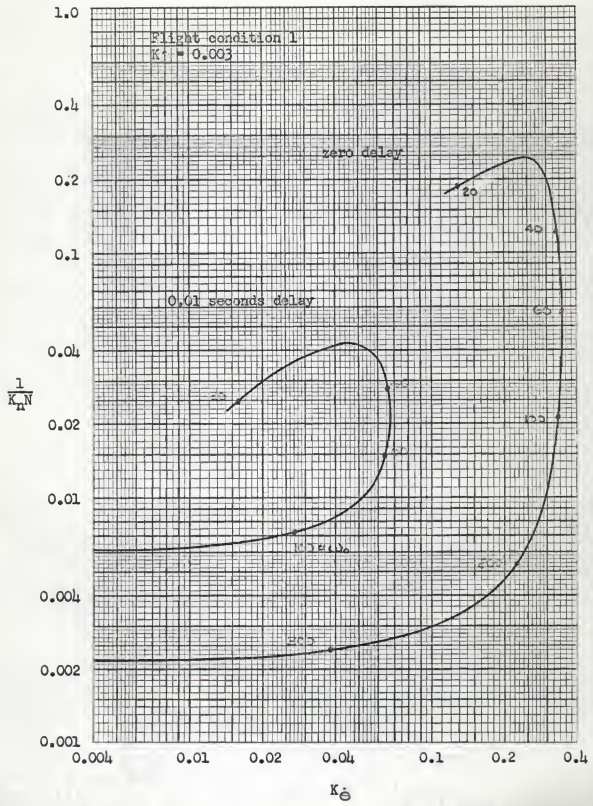

Fig. 14 Stability boundary illustrating influence of actuator delay on system stability.

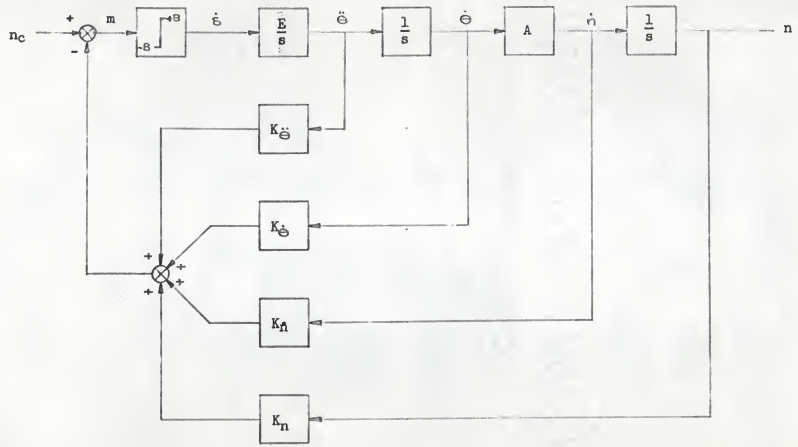

Fig. 15 Block diagram of simple airframe autopilot.

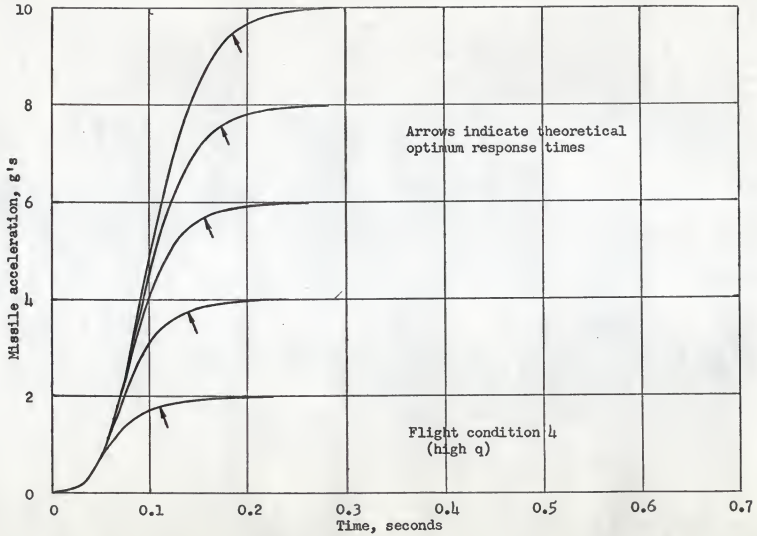

Fig. 16 Time response traces from analog computer simulation of simple airframe optimum system.

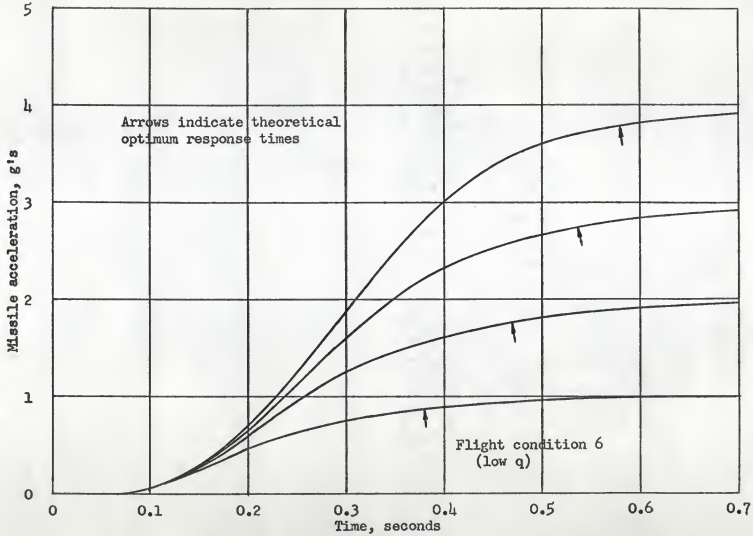

Fig. 17 Time response traces from analog computer simulation of simple airframe optimum system.

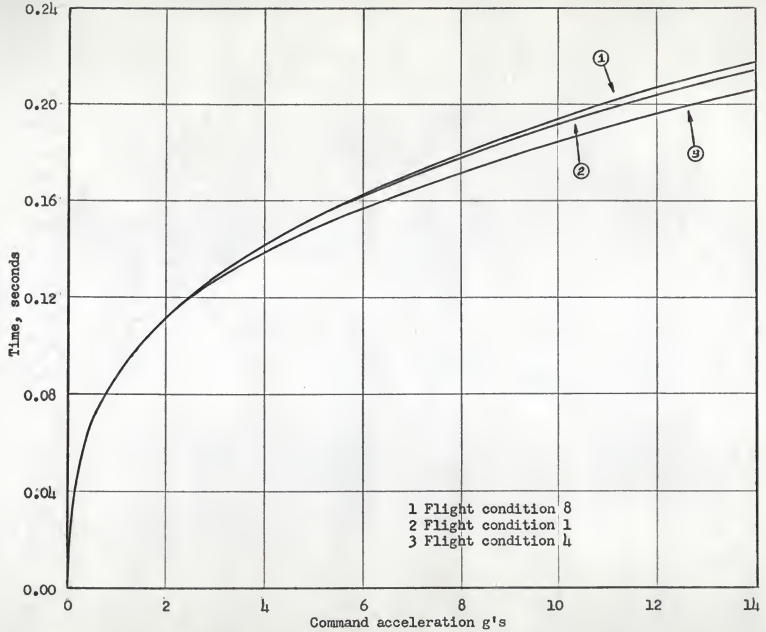

Fig. 18 Optimum response time under high q conditions.

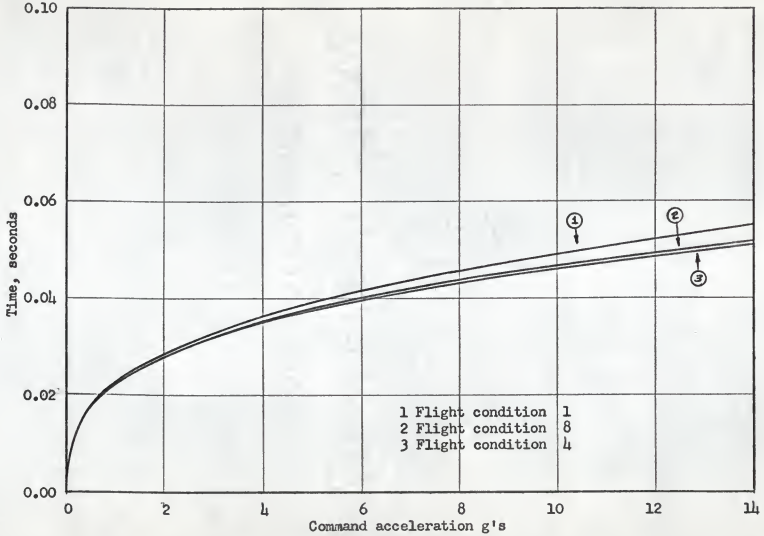

Fig. 19 Optimum first reversal time under high q conditions.

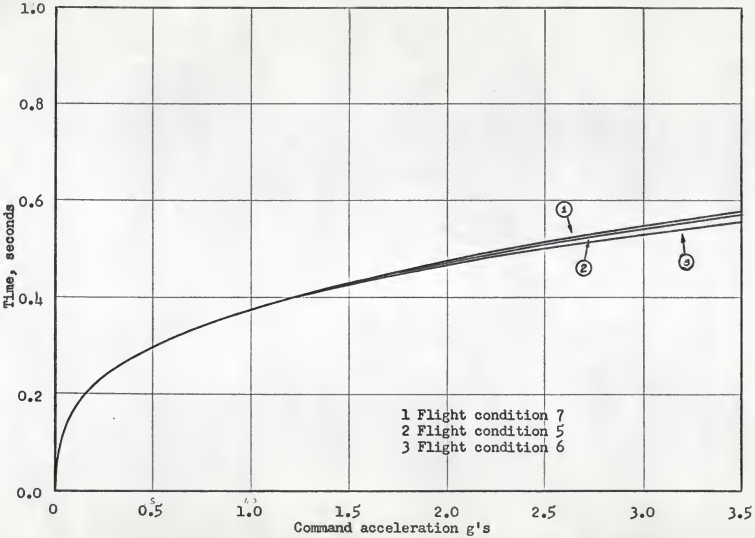

Fig. 20 Optimum response time under low q conditions.

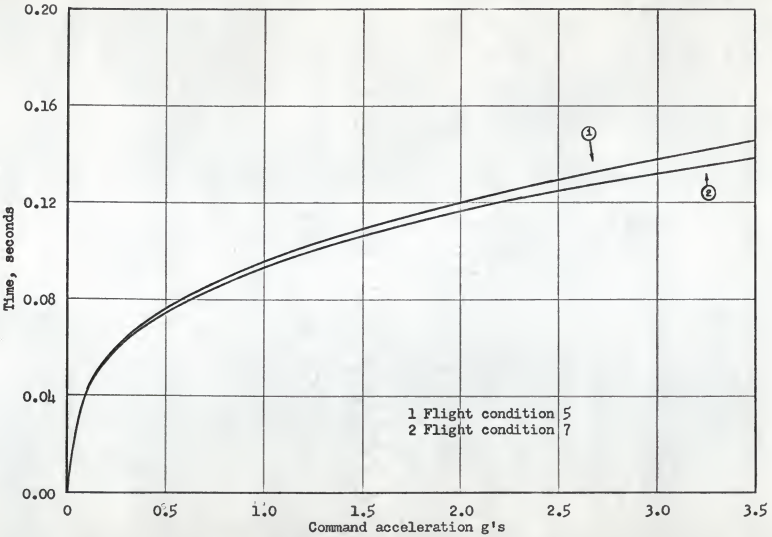

Fig. 21 Optimum first reversal time under low q conditions.

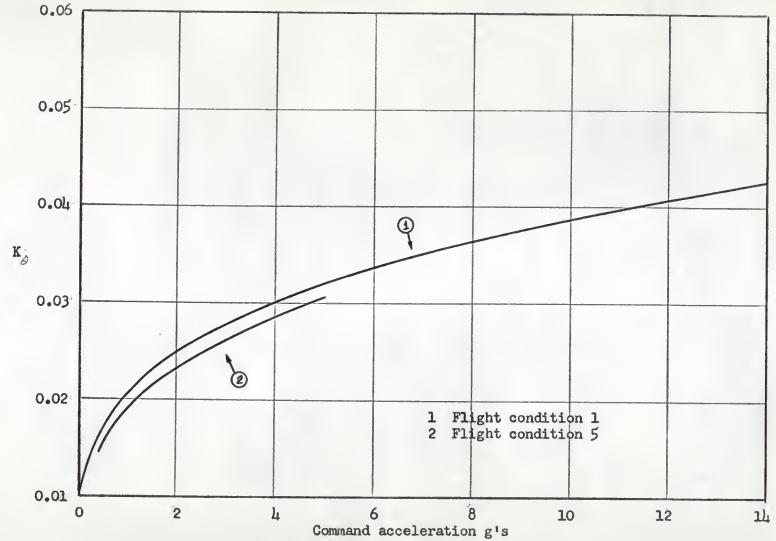

Fig. 22 Optimum values of $K_{\dot{\theta}}$ as a function of command acceleration for two flight conditions.

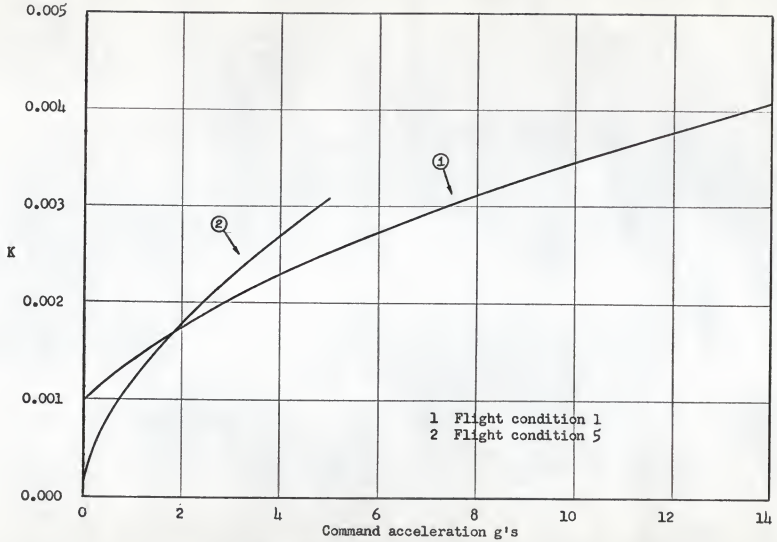

Fig. 23 Optimum values of K as a function of command acceleration for two flight conditions.

APPENDIX A

The missile airframe, which is an important part of the system discussed in this paper, is of the tail control type. Small control surfaces, located aft of the center of gravity, are used to generate turning moments on the missile body. This, in turn, rotates the body to an angle of attack such that the body forces provide the required lateral acceleration.

A representation of this airframe for control system analysis purposes, due to Amsler, is shown in the simple block diagram of Fig. 1-A. The representation used here assumes that perturbations about a trim condition are defined by the linear equations:

$$\ddot{\theta} = E\delta + C\alpha$$

$$\dot{\alpha} - \dot{\theta} - \dot{\gamma} = \dot{\theta} - n\bar{K}$$

$$n = A\alpha + D\delta$$

For certain trim conditions and very large perturbations, the airframe behavior may depart significantly from linearity. A study of system behavior for nonlinear aerodynamics is beyond the scope of this paper.

Working directly from Fig. 1-A, one finds the following airframe transfer functions:

$$\frac{n}{\dot{\delta}} = \frac{Ds^2 + \Delta}{s(s^2 + A\bar{K}s - C)} \qquad (A\text{-}1)$$

$$\frac{\dot{\theta}}{\dot{\delta}} = \frac{Es + \bar{K}\Delta}{s(s^2 + A\bar{K}s - C)} \qquad (A\text{-}2)$$

$$\Delta = AE - DC$$

In general, D is very small and may be neglected. For various airframe stability conditions and for D = 0 Eq. (A-1) becomes:

$$\frac{n}{\dot{\delta}} = \frac{AE}{s(s^2 + A\bar{K}s - C)} \qquad \text{(Stable airframe)}$$

$$\frac{n}{\dot{\delta}} = \frac{AE}{s^2(s + A\bar{K})} \qquad \text{(Neutrally stable airframe)}$$

$$\frac{n}{\dot{\delta}} = \frac{AE}{s(s + a_1)(s + a_2)} \quad \begin{matrix} a_1 > 0 \\ a_2 < 0 \end{matrix} \qquad \text{(Unstable airframe)}$$

$A = C_{N_\alpha}\, qs/mg$

$D = C_{N_\delta}\, qs/mg$

$E = C_{M_\delta}\, qsd\ 57.3/I$

$C = C_{M_\alpha}\, qsd\ 57.3/I$

$\bar{K} = 57.3 \times g/V_m$

C_M = moment coefficient

C_N = normal force coefficient

$C_{N_\alpha} = \frac{\partial C_N}{\partial \alpha}$

$C_{N_\delta} = \frac{\partial C_N}{\partial \delta}$

$C_{M_\alpha} = \frac{\partial C_M}{\partial \alpha}$

$C_{M_\delta} = \frac{\partial C_M}{\partial \delta}$

q = dynamic pressure

s = reference area

d = reference length

m = airframe mass

I = moment of inertia about center of gravity

V_m = missile velocity

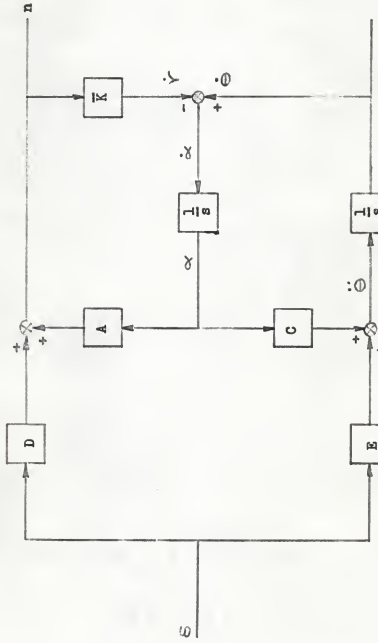

Fig. 1-4 Airframe block diagram for linear aerodynamics.

APPENDIX B

Stability b oundary data presented in this paper were computed using the IBM 1620 computer operating with a Fortran program. The source statments for this problem along with computer variables definition in terms of system variables are listed below.

```
    1 READ 2, A, B, C, E, FKBAR, TG, DG, TA, DA, FK1
    2 FORMAT (F7.3, F7.3, F7.0, F7.0, F7.1, F7.5, F7.1, F7.5,
                F7.1, F7.1)
    3 READ 4, FK2, FK3, TPR, FK
    4 FORMAT (F7.5, F7.5, F7.5, F7.5 )
    5 PUNCH 6
    6 FORMAT (47H  A  B  C  E  KBAR  K2  K3)
    7 PUNCH 8, A, B, C, E, FKBAR, FK2, FK3
    8 FORMAT(F7.3, F7.3, F7.3, F7.3, F7.3, F7.3, F7.3)
      V = TA**2
      X = TG**2
      Y = DA*TA
      Z = DG*TG
      ALPHA = V*X
      BETA = 2.*(Z*V+Y*X)
      GAMMA = V+X+4.*Y*Z)
      RHO = 2.*(Y+Z)
      DELTA = A*E-B*C
      THETA = 2.*FKBAR*DELTA*Y+E
      PI = FKBAR*DELTA*V+2.*Y*E
      PHI = E*V
      FMU = 2.*Z
      FK4 = FK*FK2
      K = 0
      W = 1.
```

```
 30 WW = W**2
    TMPA = X*WW-1.
    TMPB = B*WW-DELTA
    TMPC = PHI*WW-THETA
    TMPD = PI*WW-FKBAR*DELTA
    TMPE = TMPA*TMPB
    TMPF = FMU*W*TMPB
    TSIN = SINF(W*TPR)
    TCOS = COSF(W*TPR)
    A11 = -(BETA+A*FKBAR*ALPHA)*WW**3+(FHO+A*GAMMA*
          FKBAR-C*BETA)*WW*WW
    A12 = -(A*FKBAR-RHO*C)*WW
    A1 = A11 + A12
    B1 = TMPC*WW*TCOS-W*TMPD*TSIN
    C11 = FK4*W(TMPF*TCOS+TMPE*TSIN) -FK2*
          (TMPD*TCOS+W*TMPC*TSIN)
    C12 = FK1*(TMPE*TCOS-TMPF*TSIN)
    C1 = C11 + C12
    A22 = W*(-ALPHA*WW**3+(GAMMA+A*FKBAR*BETA-C
          *ALPHA)*WW*WW)
    A23 = -(1.+RHO*A*FKBAR-C*GAMMA)*WW*W-C*W
    A2 = A22 + A23
    B2 = W*(-TMPD*TCOS-W*TMPC*TSIN)
    C22 = FK4*W*(TMPE*TCOS-TMPE*TSIN) + FK2*W*
          (-TMPC)*TCOS + TMPD*TSIN)
    C23 = -FK1*(TMPF*TCOS+TMPE*TSIN)
    C2 = C22 + C23
    DNOM = A1*B2-A2*B1
    IF(DNOM) 100, 200, 100
100 RECN = (B1*C2-B2*C1)/DNOM
    IF(RECN) 200, 200, 110
```

```
110  FK5 = (A2* C1-A1* C2 ) /DNOM
     B3 = FK3* B1+FK1*(TMPE* TCOS- TMPF* TSIN )
     C3 = FK* W*(TMPF* TCOS+TMPE* TSIN )-(TMPD* TCOS
          +W* TMPC* TSIN)
     B4 - FK3* B2-FK1*(TMPF* TCOS+TMPE* TSIN )
     C4 = FK* W*(TMPE* TCOS- TMPF* TSIN )+(W*
          (-TMPC )* TCOS+TMPD* TSIN )
     NDOM1 = A1* C4-A2* C3
     IF(FK5) 200, 200, 120
120  IF(DNOM1) 121, 200, 121
121  RECN1 = (B4* C3-B3* C4 )/ DNOM1
122  FK6 = (A2* B3-A1* B4) / DNOM1
123  K = 1
     PUNCH 94, W, RECN, FK5, RECN1, FK6
 94  FORMAT (F6. 1, F12. 5, F12. 5, F12. 5, F12. 5 )
150  IF(W-14. 5) 152, 152, 153
152  W = W + . 5
     GO TO 30
153  IF(W - 1. 65/TPR ) 154, 300, 300
154  W = W = 5.
     GO TO 30
200  IF(K ) 300, 150, 300
300  CONTINUE
     GO TO 3
     END
```

Computer variable	System variable
TA	T_a
TG	T_g
DA	ζ_a
DG	ζ_g
FKBAR	$\bar{K}$
FK4	$K_{\dot{n}}$
FK	K_r
FK2	$K_{\dot{\theta}}$
W	ω
B	D
TPR	τ
FK3	$K_{\ddot{\theta}}$
FK5	Computed $K_{\dddot{\theta}}$
FK6	Computed $K_{\ddot{\theta}}$

ANALYSIS OF AN AUTOPILOT WITH SATURATING TYPE NONLINEAR ELEMENT

by

CLYDE HOWARD SPRAGUE

B. S., Kansas State University, 1958

AN ABSTRACT OF A MASTER'S THESIS

submitted in partial fulfillment of the

requirements for the degree

MASTER OF SCIENCE

Department of Mechanical Engineering

KANSAS STATE UNIVERSITY
Manhattan, Kansas

1963

This thesis presents a method of analyzing a nonlinear control system to determine both stability and response. The stability analysis is carried out in the frequency domain, and the response analysis is treated in the time domain. For the specific system of the type discussed in this paper, these methods are complementary. Typical numerical data, obtained by using these methods, are presented.

The autopilot on which the analysis is carried out consists of an aerodynamic vehicle with control surfaces driven by bang-bang type actuators with transportation lag. The aerodynamic loop is closed with two sensing instruments in each steering plane; an angular rate gyro and a lateral accelerometer. These instruments are coupled with appropriate mixing and shaping networks to yield a system which does not require air data scheduling.

Describing function methods are applied to the autopilot loop to yield an approximate characteristic equation. From this equation, stability surfaces in a parameter three space which define the possible oscillatory modes are derived. Root locus methods are used to interpret these surfaces and to determine what parts of the three space are acceptable operating regions. It is shown that the upper portion of the stability surface is an unsafe boundary and must be avoided. The lower portion of the surface defines a steady limit cycle oscillation which linearizes the control loop for small signals. Using the coordinates of an operating point on this part of the surface

and linear theory, one may find the small signal response of the autopilot loop.

Numerical stability data for a set of typical flight conditions and feedback parameters are shown. In addition, sets of data are presented to show the influence of airframe stability and actuator delay on the overall loop stability.

For large signals the limit cycle oscillation is suppressed throughout most of the transient period. During this time, the nonlinear element behaves as a switch or limiter and is treated as such. Optimum response for a switch type controller is assumed to exist and the theory of Laplace transforms used to find this optimum solution. Using these data, feedback networks may be designed which will yield the assumed optimum response. For a simplified airframe representation analytical expressions are developed for the feedback parameters. A numerical procedure for designing the feedback networks for a complex airframe is suggested. The influence of airframe stability on the optimum bang-bang solution is pointed out.